Phasing segmented telescopes with long-exposure phase diversity images

Serge Meimon[a,b], Enguerran Delavaquerie[a,b], Frédéric Cassaing[a,b], Thierry Fusco[a,b], Laurent M. Mugnier[a,b], Vincent Michau[a,b]

[a]Office National d'Études et de Recherches Aérospatiales
Département d'Optique Théorique et Appliquée
BP 72, F-92322 Châtillon cedex, France
[b]Groupement d'Intérêt Scientifique PHASE (Partenariat Haute résolution Angulaire Sol Espace)
between ONERA, Observatoire de Paris, CNRS and University Denis Diderot Paris 7

ABSTRACT

One of the major issues in new Extremely Large Telescopes is the phasing of their primary segmented mirror. A cophasing sensor is mandatory to achieve the ultimate resolution of the telescope. Phase diversity (PD) is a light-hardware cophasing technique. In this paper, we show that this technique is suited to segmented pupil instruments, such as the E-ELT.

Keywords: Phasing, ELT, phase diversity

1. INTRODUCTION

The first large optical telescope with a segmented mirror was the ten-meter Keck Telescope. Its primary mirror consisted of 36 hexagonal segments. All currently envisaged extremely large optical telescopes will have segmented primary mirrors, but with a much larger number of hexagonal segments, of the order of one thousand or more. To reach its optimal capabilities, the turbulent effects have to be compensated for, and the segmented primary has to be aligned, *i.e.* cophased. Whereas turbulent effects are fast evolving continuous phase screens, cophasing errors correspond to slowly evolving (compared with turbulence), discontinuous phase screens.

Therefore, cophasing requires a specific wave front sensor (WFS), although classical wave front sensors used for turbulence correction are a major source of inspiration. Among the latter, the Shack-Hartmann sensor is probably the most popular. Indeed, the sensor used for the Keck Telescope cophasing is a slightly modified Shack-Hartmann.[1] However, it is a pupil plane technique, analyzing the local derivative of the phase. Each lenslet has to be centered on an inter-segment border, to measure the differential phase between the two segments. This method does not work if one of the two segments is widely obstructed (for instance because of the spider obscuration) or missing.

This led us to propose a focal plane method, namely phase diversity, which can handle a wider kind of pupil configurations. The principle is recalled in section 2. We consider two operational cases. In the first one, the phasing sensor is located downstream a high performance Adaptive Optics (AO) system, so we consider a negligible residual turbulence and aim for extreme performance, *i.e.* a residual cophasing error below a hundredth of wavelength (section 3). The second case is less demanding in terms of residual phase error, but requires sensing phasing errors among microns of turbulence. The impact of residual turbulence on phase diversity performance is addressed in section 4.

2. PHASE DIVERSITY IN THE ELT CONTEXT

The large variety of WFSs can be classified into two families: pupil-plane sensors (such as the Hartmann-Shack and the curvature sensors) and focal-plane sensors. The focal-plane family of sensors was born from the very natural idea that an image of a given object contains information not only about the object, but also about the wave-front. A focal-plane sensor thus requires little or no optics other than the imaging sensor.

Estimating the aberrations ϕ_a from a single focal-plane image of a point source is a difficult problem known as phase retrieval.[2] Phase-retrieval has two major limitations. Firstly, it only works with a point source. Secondly, there is generally

Further information: meimon@onera.fr

a sign ambiguity in the recovered phase, i.e., the solution is not unique. Gonsalves[3] showed that by using a second image with an additional known phase variation ϕ_d with respect to the first image such as defocus, it is possible to estimate the unknown phase even when the object is extended and unknown. Figure 1 shows a scheme of such a device.

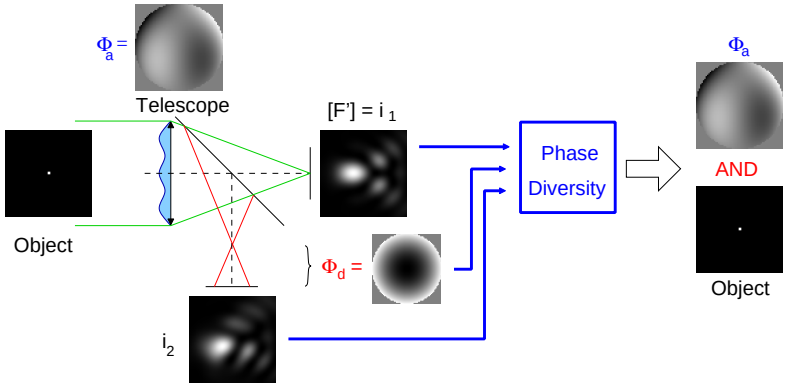

Figure 1. Phase diversity scheme.

The presence of this second image additionally removes the above-mentioned sign ambiguity of the solution. This technique, referred to as phase diversity, has been significantly developed in the past twenty years, both for wave-front sensing and for imaging (see for instance ref. 4 for a review). The data model is given by,

$$\begin{aligned} i_1 &= (o * h_1) + n_1 \quad \text{with} \quad h_1 = |TF^{-1}\{P.e^{j\phi_a}\}|^2, \\ i_2 &= (o * h_2) + n_2 \quad \text{with} \quad h_2 = |TF^{-1}\{P.e^{j(\phi_a+\phi_d)}\}|^2. \end{aligned} \tag{1}$$

The images (i_1 and i_2) are the convolution ($*$) of the source intensity distribution o and the point spread function, plus noises (photon, detector...). P is the pupil function, ϕ_d the introduced defocus and ϕ_a the phase to retrieve. This non-linear problem can be solved using a maximum *a posteriori* method consisting in choosing the object o and the phase ϕ_a which minimize a criterion $\mathcal{L}$. In the Fourier domain, we get :

$$\mathcal{L}(\boldsymbol{\phi}_a, \boldsymbol{o}) = \sum_{\boldsymbol{u}\in\mathcal{D}} \left[\frac{1}{2\sigma_1^2} |\widetilde{i_1}(\boldsymbol{u}) - \widetilde{h_1}(\boldsymbol{\phi}_a, \boldsymbol{u})\widetilde{o}(\boldsymbol{u})|^2 - \frac{1}{2\sigma_2^2} |\widetilde{i_2}(\boldsymbol{u}) - \widetilde{h_2}(\boldsymbol{\phi}_a, \boldsymbol{u})\widetilde{o}(\boldsymbol{u})|^2 \right], \tag{2}$$

where σ_1^2 and σ_2^2 are the variances associated to the images $\boldsymbol{i_1}$ et $\boldsymbol{i_2}$ (supposed equal in the following). The sum is computed on the support of the OTF, the frequency domain $\mathcal{D}$.The minimization of $\mathcal{L}$ is performed alternately with respect to the object and with respect to the aberrations.

A major asset of Phase Diversity when cophasing a segmented telescope is linked to its focal-plane nature. Indeed the images are the results of the diffraction of the light on the apertures to be tested. Because each aperture interferes with all the others, the presence of missing segments or a wide spider (figure 2) does not yield major changes. One only has to inform the algorithm about the actual pupil configuration, corresponding to the pupil term P of equation (1).

3. PHASE DIVERSITY WITHOUT TURBULENCE

We performed a simulation of the method in an E-ELT configuration, to measure the accuracy in function of the number of photons (fig. 3).The detector read-out noise (RON) is 5 photo-electrons. The photon noise regime is very clear on the graphic. Assuming a spectral bandwidth worth $40nm$, and a G0 star of magnitude 12 source object, we compute the number of incoming photons ($10^8/s$) in the visible, *i.e.* at $\lambda = 650nm$, and in the infrared ($1.4 \times 10^7/s$), *i.e.* at $\lambda = 1300nm$. The residual phasing error is then equal to $4nm$ in the visible, and $20nm$ in the infrared for an integration time of 1 second. Because our software cannot yet handle 2π wrapping, we use an input phasing error worth $\lambda/20$ rms. The input and residual phasing error maps are shown in fig. 4. These simulations correspond to a random piston input error. We performed the same simulations with tip, tilt and piston and obtained similar results.

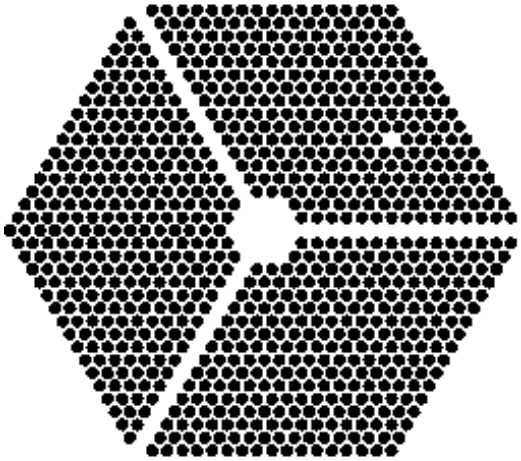

Figure 2. Spider masked pupil, with a missing segment.

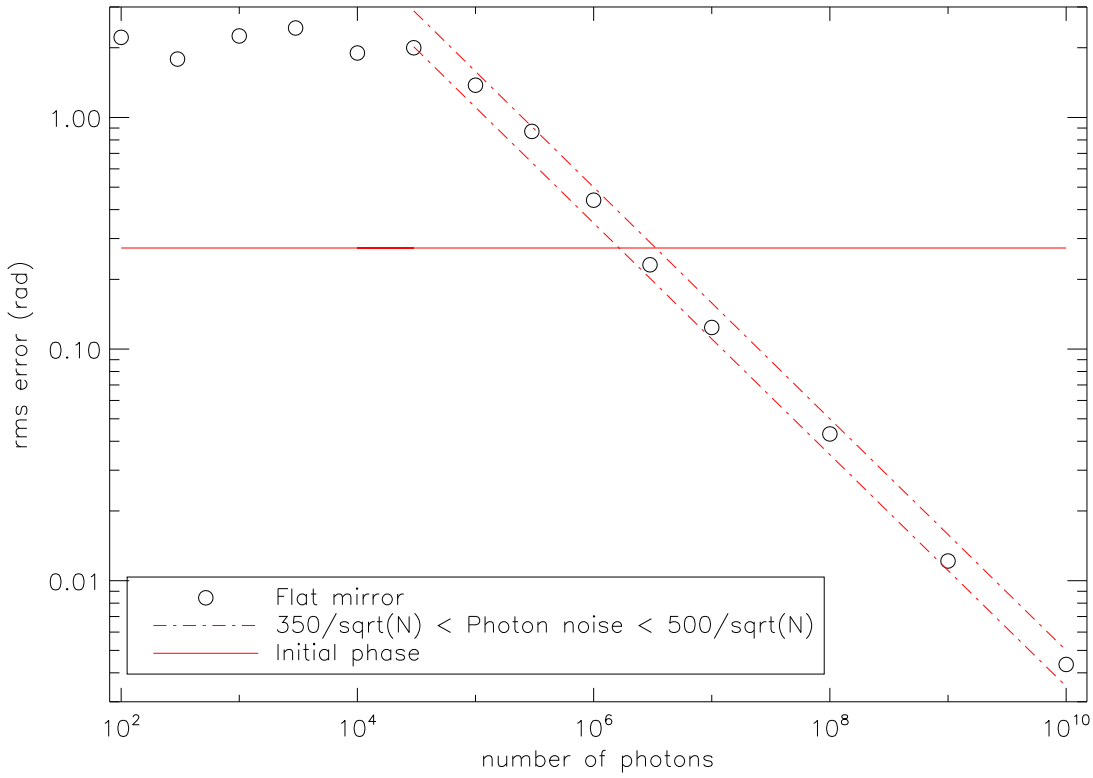

Figure 3. Residual phasing error in function of the number of incoming photons. In the photon noise regime, the error scales in $\alpha/\sqrt{N_{phot}}$, with α between 350 and 500.

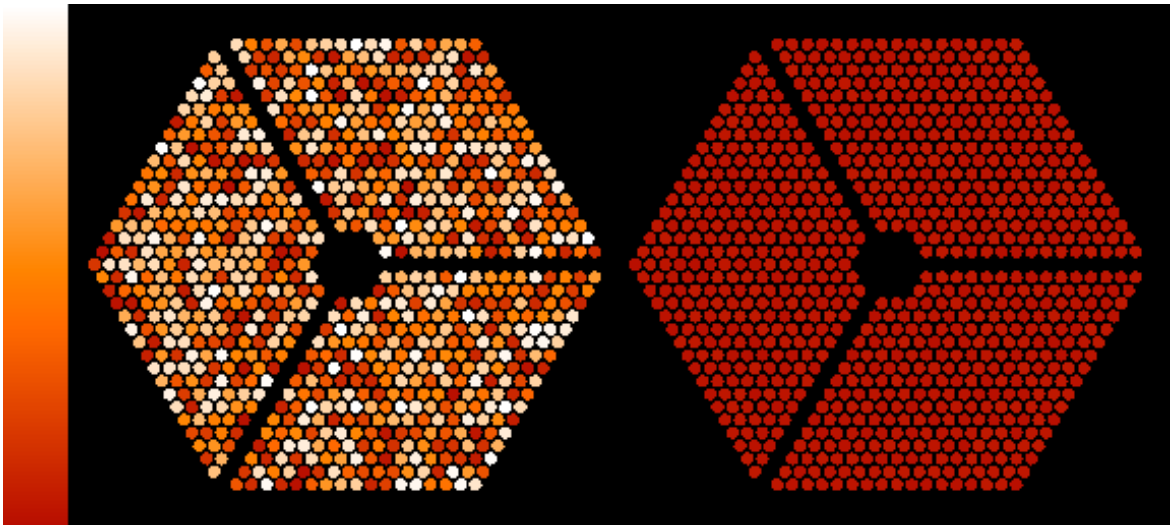

Figure 4. Input (Left) and residual (right) phasing error maps, for 1s integration on a magnitude 12 G0 star, in the visible.

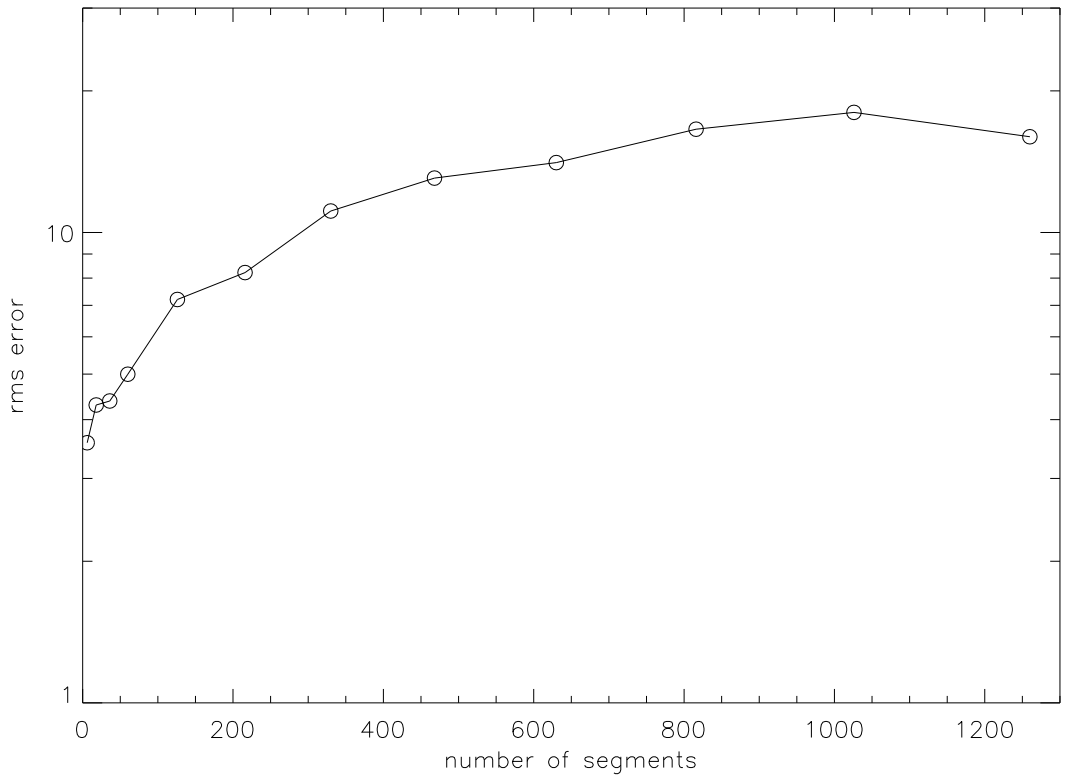

Figure 5. Phasing error in photon noise regime vs number of segments. The number of photons per segment is constant.

To assess the impact of the number of modes to estimate, we have studied the phasing error in photon noise regime with a varying number of segments, assuming a constant amount of photons per segment (fig. 5).

The error increases with the number of modes to retrieve, but this trend is partly compensated by the increase in the number of photons. However, our algorithm was wrote originally to process three segments data. By optimizing it for the E-ELT case, we should obtain at least a constant curve.

As emphasized in fig. 4 left, the input phasing error has very high spatial order components. Conversely, atmospheric turbulence corrugations and optical flatness error contain mainly low-order Zernike modes.[5,6] This led to question the choice of a Z_4 diversity phase, *i.e.* the use of a defocalized plane, in the context of a phasing error. It is likely that a Z_4 diversity phase will be highly sensitive to low-order modes, whereas a higher-order diversity phase should be more accurate on sensing high-order aberrations.

A Z_4 diversity phase is usually chosen because it is easily implemented on an optical bench. However, it is possible to use deformable mirrors or phase screens to obtain another diversity phase. A way to pick the "right" diversity phase is to measure the sensitivity of the criterion to the aberrations, in function of the diversity phase used. To do so, we compute the Hessian matrix of the criterion (as in[7]). The diagonal components reflect the sensitivity of the criterion for each Zernike mode of the aberration to determine. This Hessian diagonal vector can be computed for a Z_4 diversity phase as well as for any other mode. We computed these for a Z_4 diversity phase (fig.6),and for a Z_{172} diversity phase (fig.7). The X-coordinates are the indices of the Zernike mode of the aberration to measure.

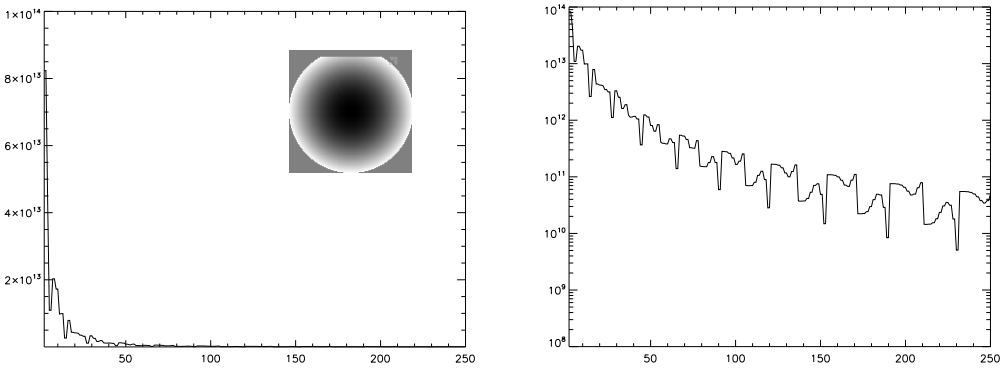

Figure 6. Hessian diagonal components, for a Z_4 diversity phase, in linear (left) and log (right) scales.

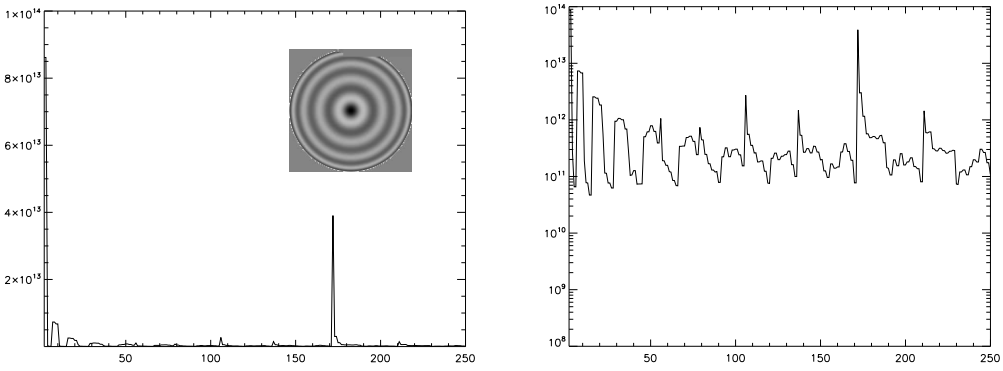

Figure 7. Hessian diagonal components, for a Z_{172} diversity phase, in linear (left) and log (right) scales.

We can see that phase diversity with a defocalized plane will be sensitive mainly to the focus, whereas a Z_{172} diversity phase apparatus will analyze accurately a Z_{172} aberration* (see figs. 6, 7). In both cases, phase diversity is sensitive to

*Note however that an error in the diversity phase measurement is totally transfered to the phase estimation error, e.g. asuming a 1 radian diversity phase with an actual phase of 2 radians would yield a 1 radian focus estimation error.[8] In other words, even if a Z_n diversity phase is the optimal choice to analyze a pure Z_n, the sensor thus obtained would be extremely sensitive to model errors.

the other modes with same radial order, but decreasingly with the azimuthal order. This might be an explanation why a defocalized plane is generally used to measure aberrations on full pupils affected by turbulence and optical components surface errors: its sensitivity to the various Zernike modes has the same profile as the average decomposition of the aberrations to analyze.

The segmentation of an ELT primary mirror yields a different order decomposition of the average perturbation : a random set of segment tip/tilt/piston aberration is analogous to a white noise, *i.e.* it contains as much low order modes as high order modes. Figs. 6, 7 correspond to a circular aperture. With an hexagonal configuration with gaps between segments, the Hessian diagonal components for a Z_4 or a Z_{172} diversity phase, is modified (see figs. 8, 9).

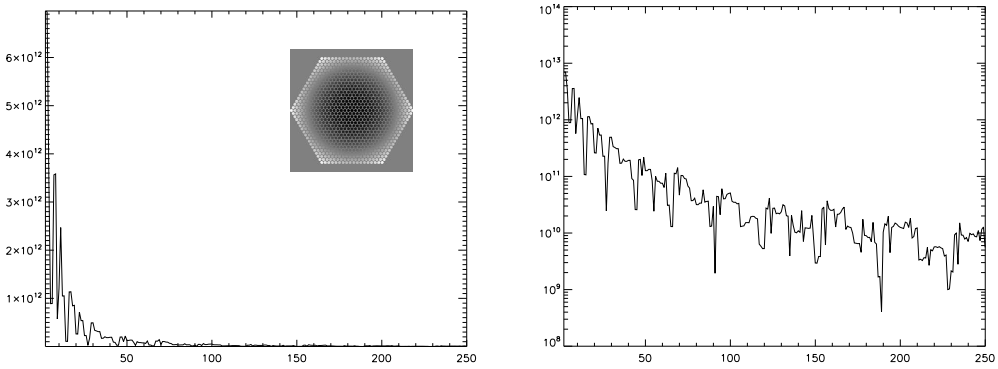

Figure 8. Hessian diagonal components, for a Z_4 diversity phase with a segmented pupil mask, in linear (left) and log (right) scales.

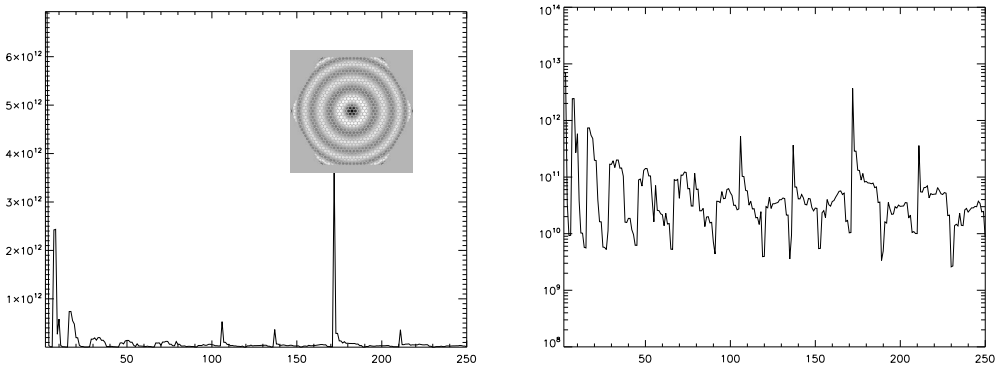

Figure 9. Hessian diagonal components, for a Z_{172} diversity phase with a segmented pupil mask, in linear (left) and log (right) scales.

By comparing the two profiles (fig. 10), we see that a Z_4 diversity phase is more sensitive to low order modes, whereas a Z_{172} diversity phase yields a more homogeneous profile, although slightly more sensitive to high order modes. Therefore, we expect a better correction by using Z_{172}.

We performed simulations with a diversity phase other than focus, for instance, Z_{37} and Z_{172}. In order to characterize the structure of the residual phasing error, we plot the rms phasing error for each corona of the E-ELT primary mirror (fig. 11), for the three aforementioned diversity phases.

These result tend to prove that a high order Zernike mode diversity phase is more efficient. With a Z_{172}, the rsm error is divided by 5, which means that a sub-nanometric accuracy is doable with a 5 seconds integration time.

4. PHASE DIVERSITY WITH TURBULENCE

Because phasing will have to be done regularly, probably more than once a day, it will need to be done on sky. The images from which the phase diversity has to retrieve the phasing errors are therefore affected by the atmospheric turbulence. Two options are possible:

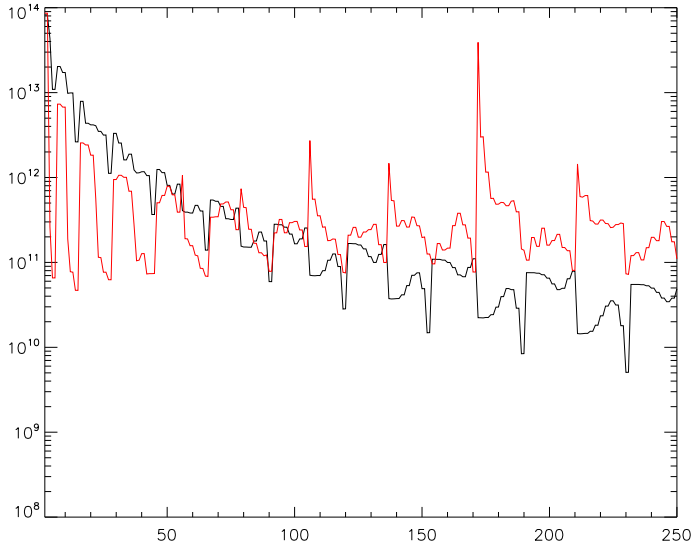

Figure 10. Hessian diagonal components, for a Z_4 diversity phase (black),and for a Z_{172} diversity phase (red)

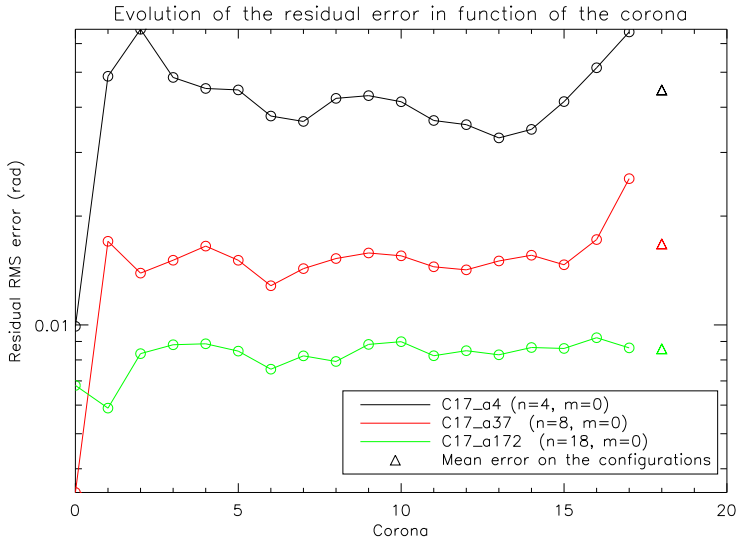

Figure 11. Rms phasing error for each corona of the E-ELT primary mirror, for three different diversity phase.

- Measuring the total phase error, including turbulence and phasing error, on short exposure data (with a typical integration time worth a few milliseconds), and averaging the measurements to cancel out the turbulence contributor (supposed to be 0 mean);
- Averaging the turbulence before measuring the phase, *i.e.* trying to retrieve the phasing error from long-exposure images.

The first option is not realistic considering reference stars of magnitude higher than 12. In the second option, if the exposure is long enough, the impact of turbulence is similar to a supplementary Optical Transfer Function (OTF),[9] which tends to smooth the point spread function (PSF). As identified by Mugnier et. al., the Phase Diversity algorithm will take this turbulent OTF into account as a part of the object:[10]the data model is exactly the same as if the observed source was a point source convolved with the turbulent OTF, and if the only aberrations were the static part, *i.e.* the phasing error. On this basis, we performed the same simulations as before, but with an object equal to a point source convolved with the turbulent OTF. The typical width of the object depends on the turbulent phase variance. Fig. 12) plots for various turbulent phase variances the estimation rms error of the Phase Diversity algorithm.

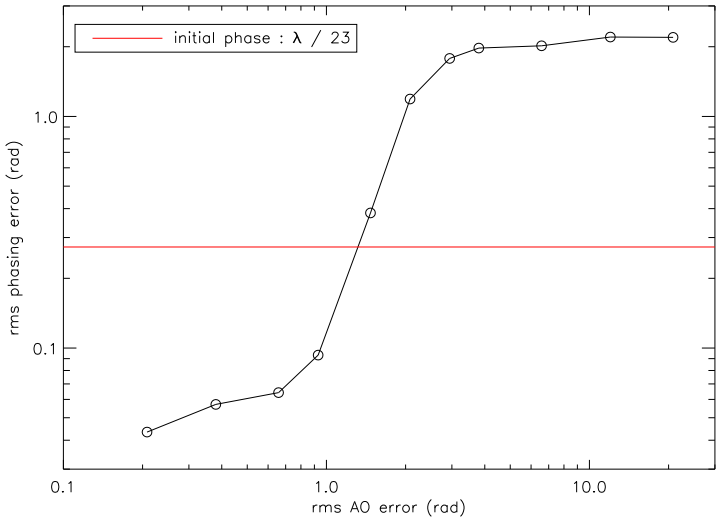

Figure 12. Phase Diversity algorithm estimation rms error versus turbulent phase standard deviation

The input phasing error being $\lambda/20$, the phasing error is amplified for turbulent phase variance higher than a few squared radians. We can then formulate the following criterion : our phase diversity algorithm performs correctly only if the Adaptive Optics (AO) system residual error is worth 1 radian rms or less.

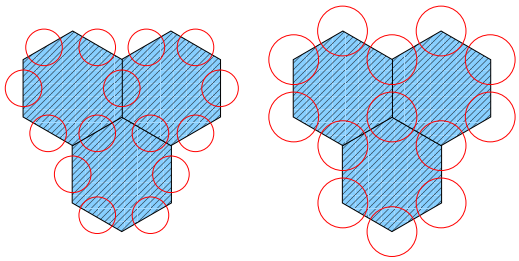

Figure 13. “Edge” and “vertex” configurations.

Without AO correction, the turbulent phase variance is worth 1 squared radian over any r_0 diameter sub pupil, by definition of r_0. In this case, we have to set the lenslet diameters to r_0, and use phase diversity on each one. The design obtained is then very close to Keck’s Shack-Hartmann wavefront sensor. However, Phase Diversity can handle any kind

of pupil, and is therefore less sensitive to lenslet misalignments, for example. It also allows a "vertex" configuration (see fig. 13 right) instead of a classical "edge" configuration (see fig. 13 left).

In a "vertex" configuration, each lenslet is across three segments. Even if one segment is missing, the remaining flux in the lenslet is not lost, it can still be used to cophase the two remaining segments.

With a Ground Layer Adaptive Optics (GLAO) correction, the zone within which the AO residual error is worth 1 radian rms or less gets wider, reaching a few r_0 diameter. If its diameter is equal to a segment edge length or more, then the vertex configuration is optimal: all lenslets will be tangential. In this case, because the "vertex" configuration is more compact, it will collect one third of the flux more than the "edge" one.

With an Extreme AO system, the residual phase error is below 1 radian rms over the whole pupil, and results of section 3 apply. We believe that phase diversity in this case has a great potential:

- it is almost hardware free:actually, it is often already present in an optical bench, because it requires only a focal image and a slightly defocalized image. The precise knowledge of the amount of defocus introduced is very critical.
- it is suited to extreme performance designs with no or little turbulence : its accuracy has been experimentally demonstrated for high performance calibration on a monolithic pupil,[11] and it is the baseline solution for the JWST space telescope fine phasing.[12]
- Our simulations tend to prove that it should also apply to an ELT pupil configuration. Moreover, the use of an optimally designed diversity phase should allow to reach even higher performance.

5. CONCLUDING COMMENTS

We have studied the use of phase diversity in the case of a phasing sensor located downstream a high performance Adaptive Optics (AO) system, *i.e.* with a negligible residual turbulence. We have shown that a residual cophasing error below a hundredth of wavelength (section 3) is reachable with reasonable integration times (typically a few seconds). To do so, we have proposed the use of a specifically designed diversity phase, and shown the corresponding gain compared to a classical defocus.

When dealing with a partially corrected turbulence, we have derived a working domain for phase diversity and proposed an original "vertex" lenslet configuration.

The results presented here are only preliminary. For instance, we hope to obtain a formal derivation of the diversity phase optimal for a given aberration power spectrum density. In future months, we also plan to process experimental data from the APE experiment.[13]

As regards turbulent effects, we have considered an infinitely long exposure, which is of course restrictive. However the limitations of the work presented here, we believe it provides promising guidelines and concepts.

REFERENCES

[1] G. Chanan, M. Troy, F. Dekens, S. Michaels, J. Nelson, T. Mast, and D. Kirkman, "Phasing the mirror segments of the Keck telescopes: the broadband phasing algorithm.," Appl. Opt. **37,** 140–155 (1998).

[2] R. A. Gonsalves, "Phase retrieval from modulus data," J. Opt. Soc. Am. **66,** 961–964 (1976).

[3] R. A. Gonsalves, "Phase retrieval and diversity in adaptive optics," Opt. Eng. **21,** 829–832 (1982).

[4] L. M. Mugnier, A. Blanc, and J. Idier, "Phase Diversity: a Technique for Wave-Front Sensing and for Diffraction-Limited Imaging," *Advances in Imaging and Electron Physics*, P. Hawkes, ed., (Elsevier, 2006), Vol. 141, Chap. 1, pp. 1–76.

[5] R. J. Noll, "Zernike polynomials and atmospheric turbulence," J. Opt. Soc. Am. **66,** 207–211 (1976).

[6] K. Dohlen, J.-L. Beuzit, M. Feldt, D. Mouillet, P. Puget, J. Antichi, A. Baruffolo, P. Baudoz, A. Berton, A. Boccaletti, M. Carbillet, J. Charton, R. Claudi, M. Downing, C. Fabron, P. Feautrier, E. Fedrigo, T. Fusco, J.-L. Gach, R. Gratton, N. Hubin, M. Kasper, M. Langlois, A. Longmore, C. Moutou, C. Petit, J. Pragt, P. Rabou, G. Rousset, M. Saisse, H.-M. Schmid, E. Stadler, D. Stamm, M. Turatto, R. Waters, and F. Wildi, "SPHERE: A planet finder instrument for the VLT," in *Ground-based and Airborne Instrumentation for Astronomy*, I. S. McLean and M. Iye, eds.,6269 (2006).

[7] R. G. Paxman, T. J. Schulz, and J. R. Fienup, "Joint estimation of object and aberrations by using phase diversity," J. Opt. Soc. Am. A **9,** 1072–1085 (1992).

[8] A. Blanc, T. Fusco, M. Hartung, L. M. Mugnier, and G. Rousset, "Calibration of NAOS and CONICA static aberrations. Application of the phase diversity technique," Astron. Astrophys. **399,** 373–383 (2003).

[9] F. Roddier, in *Progress in Optics*, E. Wolf, ed., (1981), Vol. 19.

[10] L. M. Mugnier, J.-F. Sauvage, A. Cornia, S. Dandy, and T. Fusco, "Sensing Static Aberrations of Ground-Based Telescopes by Long-Exposure Phase Diversity," Opt. Lett. (en préparation).

[11] J.-F. Sauvage, T. Fusco, G. Rousset, and C. Petit, "Calibration and Pre-Compensation of Non-Common Path Aberrations for eXtreme Adaptive Optics," J. Opt. Soc. Am. A **24,** 2334–2346 (2007).

[12] D. S. Acton, P. D. Atcheson, M. Cermak, L. K. Kingsbury, F. Shi, and D. C. Redding, in *James Webb Space Telescope wavefront sensing and control algorithms*, J. C. Mather, ed., (SPIE, 2004), No. 1, pp. 887–896.

[13] F. Gonte, N. Yaitskova, F. Derie, A. Constanza, R. Brast, B. Buzzoni, B. Delabre, P. Dierickx, C. Dupuy, R. Esteves, C. Frank, S. Guisard, R. Karban, E. Koenig, J. Kolb, M. Nylund, L. Noethe, I. Surdej, A. Courteville, R. Wilhelm, L. Montoya, M. Reyes, S. Esposito, E. Pinna, K. Dohlen, M. Ferrari, and M. Langlois, "APE: the Active Phasing Experiment to test new control system and phasing technology for a European Extremely Large Optical Telescope," in *Advanced Wavefront Control: Methods, Devices, and Applications III. Edited by Gruneisen, Mark T.; Gonglewski, John D.; Giles, Michael K. Proceedings of the SPIE, Volume 5894, pp. 306-317 (2005).*, M. T. Gruneisen, J. D. Gonglewski, and M. K. Giles, eds., Presented at the Society of Photo-Optical Instrumentation Engineers (SPIE) Conference **5894,** 306–317 (2005).